nature nanotechnology

ARTICLES

PUBLISHED ONLINE: 21 SEPTEMBER 2014 | DOI: 10.1038/NNANO.2014.199

Strong underwater adhesives made by self-assembling multi-protein nanofibres

Chao Zhong[1,2,3†], Thomas Gurry[1,4], Allen A. Cheng[1,2,3], Jordan Downey[2,3], Zhengtao Deng[1,2,3], Collin M. Stultz[1,4,5] and Timothy K. Lu[1,2,3,4*]

Many natural underwater adhesives harness hierarchically assembled amyloid nanostructures to achieve strong and robust interfacial adhesion under dynamic and turbulent environments. Despite recent advances, our understanding of the molecular design, self-assembly and structure–function relationships of these natural amyloid fibres remains limited. Thus, designing biomimetic amyloid-based adhesives remains challenging. Here, we report strong and multi-functional underwater adhesives obtained from fusing mussel foot proteins (Mfps) of *Mytilus galloprovincialis* with CsgA proteins, the major subunit of *Escherichia coli* amyloid curli fibres. These hybrid molecular materials hierarchically self-assemble into higher-order structures, in which, according to molecular dynamics simulations, disordered adhesive Mfp domains are exposed on the exterior of amyloid cores formed by CsgA. Our fibres have an underwater adhesion energy approaching 20.9 mJ m^{-2}, which is 1.5 times greater than the maximum of bio-inspired and bio-derived protein-based underwater adhesives reported thus far. Moreover, they outperform Mfps or curli fibres taken on their own and exhibit better tolerance to auto-oxidation than Mfps at pH $\geq$ 7.0.

Strong underwater adhesives are needed for technological and biomedical applications in water or high-moisture settings[1,2]. An emerging strategy for developing such advanced molecular materials is based on mimicking and improving upon naturally occurring underwater adhesives from marine organisms[2–4]. The versatility of 3,4-dihydroxyphenylalanine (DOPA) for crosslinking and coupling in natural underwater interfacial adhesion phenomena has promoted a wide range of biomimetic research efforts focused on DOPA-containing or DOPA-analogue-containing peptides[5,6], hydrogels[7], polymer constructs[3,8] and recombinant Mfp variants[9]. In contrast, the rational design of biomimetic underwater adhesives through molecular self-assembly has lagged behind, even though the importance of hierarchical assembly of protein complexes into higher-order structures is increasingly recognized in natural underwater adhesive systems[10,11].

Several marine organisms, including barnacles, algae and marine flatworms, exhibit remarkable moisture-resistant adhesion to a variety of substrata by utilizing functional amyloid nanostructures[12,13]. Amyloids are characterized by β-strands that are oriented perpendicularly to the fibril axis and connected through a dense hydrogen-bonding network, which leads to supramolecular β-sheets that usually extend continuously over thousands of molecular units[14–16]. Such fibrillar structures have intrinsic advantages for interfacial underwater adhesion. These advantages include tolerance to environmental deterioration, self-healing arising from self-polymerization, and large fibre surface areas[10,16–18], which appear to enhance adhesion by increasing the contact area in the adhesive plaques of barnacles[13]. In addition, potential mechanical benefits of amyloid nanostructures include the cohesive strength associated with the generic amyloid intermolecular β-sheet structure and adhesive strength related to adhesive residues external to the amyloid core[12,16]. Amyloid structures can therefore constitute the basis for a promising new generation of bio-inspired adhesives for a wide range of applications[3,12]. Despite advances in both amyloid self-assembly[14–16] and amyloid-enabled nanotechnology[16,19,20], the rational design of biomimetic amyloid-based underwater adhesives remains challenging and has not been demonstrated experimentally, in part due to the limited understanding of the underlying biological design principles.

We have rationally designed a new generation of bio-inspired adhesives that combine two independent natural adhesion systems, DOPA-based adhesives and amyloid-based adhesives, using synthetic-biology techniques (Fig. 1). To achieve strong interfacial underwater adhesion, we selected Mfp3 and Mfp5 (representatives of DOPA-based mussel adhesives originating from *Mytilus galloprovincialis*[2]) and CsgA (an amyloidogenic protein that is the major subunit of adhesive curli fibres in *Escherichia coli*[18]) (Fig. 1a, Supplementary Fig. 1) from an inventory of adhesive biomolecules and genes compiled over decades of molecular biology and functional genomics research. Two genetic fusion constructs, CsgA-Mfp3 and Mfp5-CsgA, were constructed using isothermal one-step Gibson DNA assembly (Fig. 1b, Supplementary Figs 2–5). Because CsgA is amyloidogenic, we reasoned that both CsgA-Mfp3 and Mfp5-CsgA would self-assemble into fibrous bundles or films with adhesive properties[19] by displaying the mussel adhesion domains on the surface of amyloid scaffolds. We further hypothesized that the co-assembly of the two fusion proteins together would lead to hierarchically assembled copolymer structures that could integrate synergistic features from the two different types of adhesive modules and potentially recapitulate the intermolecular interactions between Mfp3 and Mfp5 found in natural adhesion systems[2] (Fig. 1c,d).

[1]Department of Electrical Engineering and Computer Science, Massachusetts Institute of Technology, Cambridge, Massachusetts 02139-4307, USA, [2]Department of Biological Engineering, Massachusetts Institute of Technology, Cambridge, Massachusetts 02139-4307, USA, [3]Synthetic Biology Group, Research Laboratory of Electronics, Massachusetts Institute of Technology, Cambridge, Massachusetts 02139-4307, USA, [4]Computational and Systems Biology Initiative, Massachusetts Institute of Technology, Cambridge, Massachusetts 02139-4307, USA, [5]The Institute of Medical Engineering and Science, Massachusetts Institute of Technology, Cambridge, Massachusetts 02139-4307, USA; [†]Present address: School of Physical Science and Technology, ShanghaiTech University, Shanghai 201210, China. *e-mail: timlu@mit.edu

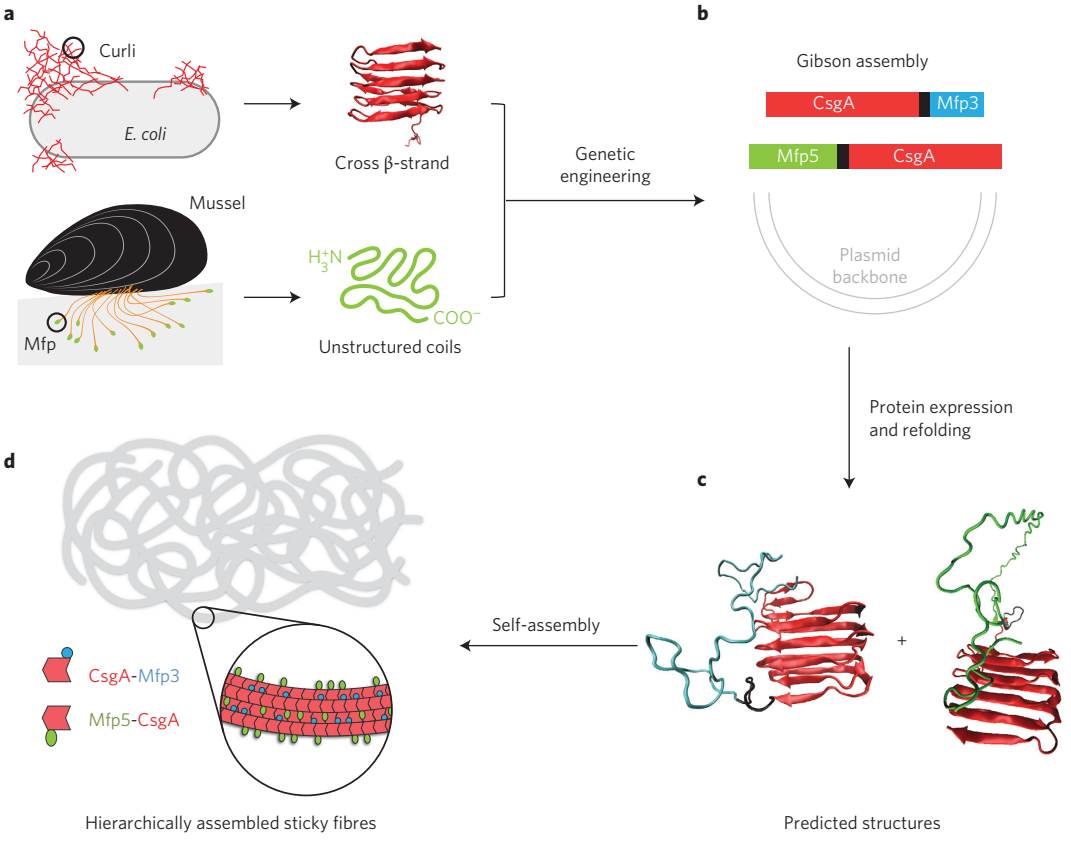

Figure 1 | Combinatorial and modular genetic strategy for engineering self-assembling underwater adhesives. a, Schematic of two independent natural adhesive proteins: curli from *E. coli* and mussel foot proteins (Mfps) from mussels. Curli are adhesive amyloid fibres composed of the major functional subunit CsgA. CsgA contains five stacked strand–loop–strand motifs mediated by conserved residues (Supplementary Fig. 1) and can self-assemble into nanofibres via a rate-limiting nucleation step followed by fibril extension[18]. Mfp3 and Mfp5, major mussel adhesive foot proteins, have unstructured coil structures in solution[32,49] and are critical to the underwater interfacial adhesion of mussels[2]. **b**, The modular design of artificial adhesive materials is enabled by rationally fusing genes encoding the two natural adhesive elements shown in **a**. Two gene constructs (CsgA-Mfp3 and Mfp5-CsgA) were independently created using one-pot isothermal Gibson assembly and tagged with poly-histidine residues to enable purification. **c**, Schematic of predicted cross-β-strand structures for CsgA-Mfp3 and Mfp5-CsgA in solution. In both predicted structures, CsgA forms the amyloid core, with Mfp3 and Mfp5 extending from CsgA's C-terminal or N-terminal, respectively, as unstructured coil structures. **d**, Because of the amyloidogenic domains, CsgA-Mfp3 and Mfp5-CsgA monomers can self-assemble into large bundles of fibrils or hierarchical networks of filaments. CsgA domains are key to fibre self-assembly by enabling fibril extension through self-polymerization and β-strand lamination by lateral stacking, with adhesive domains Mfp3 and Mfp5 exposed on the fibril surfaces. *In vitro* copolymerization of the CsgA-Mfp3 and Mfp5-CsgA monomers can lead to hierarchically co-assembled structures with two different adhesive domains displayed on amyloid scaffolds, potentially recapitulating intermolecular interactions between Mfp3 and Mfp5 molecules in natural mussel adhesion systems[2]. Enhanced underwater adhesion is expected to arise from the synergy between the high fibre surface area of curli and the adhesive residues from the Mfp domains.

Molecular dynamics and molecular characterization

To investigate whether the presence of a disordered Mfp domain would affect the overall structure of CsgA amyloid cores, we built molecular dynamics models representing both monomeric and fibrillar states of the CsgA-Mfp3, Mfp5-CsgA and (CsgA-Mfp3)-co-(Mfp5-CsgA) copolymer constructs (Fig. 2, Supplementary Fig. 6). Simulations of the monomeric proteins (1 μs) and the fibrillar states (200 ns) indicated that the core amyloid structure does not significantly diverge from that of a prototypical amyloid structure when the disordered domains are present (Fig. 2). These results suggest that CsgA-Mfp3 alone, Mfp5-CsgA alone, and copolymers of the two fusion proteins should form stable amyloid structures dominated by the CsgA domains, with the highly disordered Mfp domains displayed external to the amyloid core in all cases (Fig. 2a–c) and potentially interacting with each other in the copolymer construct (Fig. 2c).

We expressed the adhesive proteins in *E. coli*, purified them, and exposed them to the enzyme tyrosinase to convert tyrosine residues to DOPA (Supplementary Fig. 7). Hereafter, 'unmodified' and 'modified' adhesive proteins refer to the proteins before and after tyrosinase conversion. CsgA-Mfp3 (unmodified and modified) and Mfp5-CsgA (unmodified and modified) migrated as single bands at ~28.5 kDa and ~32 kDa, respectively, under SDS-polyacrylamide gel electrophoresis (SDS-PAGE), in contrast with the single band at ~17 kDa for CsgA (Fig. 3a). No clear differences were detected between the band positions of the unmodified and modified versions of the same protein based on SDS-PAGE and western blotting (Fig. 3a). However, more accurate molecular weight (M_w) assessment by matrix-assisted laser-desorption ionization time-of-flight (MALDI-TOF) showed higher values of M_w in the modified adhesive proteins (compared with their unmodified counterparts), which we attribute to the conversion of tyrosine residues into DOPA with tyrosinase modification (Fig. 3b, Supplementary Fig. 8). Based on MALDI-TOF spectra, we found that adhesive proteins collected from borate buffer had higher M_w values than those collected from acid solutions, probably due to the formation of diol-borate bonds between DOPA and borate[21], thus confirming successful modification of the adhesive proteins

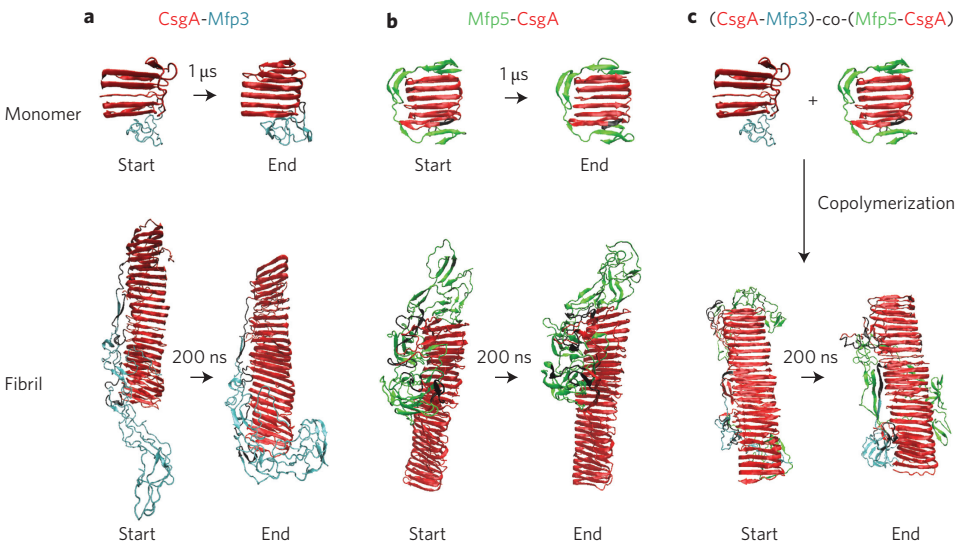

Figure 2 | Comparison of monomer, individual fibril and co-assembled fibril structures before and after molecular dynamics simulations for modified CsgA-Mfp3, Mfp5-CsgA and (CsgA-Mfp3)-co-(Mfp5-CsgA) copolymer constructs. a, Start and end simulated structures for the CsgA-Mfp3 monomer (top) and fibril (bottom). **b**, Start and end simulated structures for the Mfp5-CsgA monomer (top) and fibril (bottom). **c**, Start and end simulated structures for (CsgA-Mfp3)-co-(Mfp5-CsgA) fibril (bottom), which are assembled via copolymerization of CsgA-Mfp3 and Mfp5-CsgA (top). For both monomeric and fibrillar states of the constructs, the start and end structures display similar structures: the CsgA domains always dominate the well-ordered amyloid cores, whereas disordered Mfp5 or Mfp3 domains are external to the amyloid cores. Simulation times for monomeric and fibrillar structures were 1 μs and 200 ns, respectively.

(Supplementary Fig. 8). In addition, DOPA residues were detected in mature hybrid amyloid fibres with the nitro blue tetrazolium (NBT) staining assay; only the modified samples turned purple due to redox-cycling of DOPA residues[22] (Fig. 3c). Further quantitative analysis by acid-borate difference spectrum (ABDS) analysis[21] revealed conversion percentages from tyrosine to DOPA of 64.8% and 56.0% for modified CsgA-Mfp3 and Mfp5-CsgA, respectively (Fig. 3d, Supplementary Fig. 10), in agreement with results obtained from amino acid analysis (Fig. 3d, Supplementary Figs 12,13).

Our hybrid adhesive proteins formed hierarchically self-assembled structures (Fig. 1d). Immediately after elution from cobalt resin columns, solutions containing CsgA-Mfp3 (unmodified or modified) or Mfp5-CsgA (unmodified or modified) were clear, with no evidence of aggregation. However, after about 2 h of incubation under ambient conditions, the solutions became opaque and noticeably viscous. Transitions of soluble proteins to insoluble amyloid aggregates can be monitored using thioflavin T (ThT), an amyloid-specific dye commonly used to assay amyloid formation[23]. The ThT fluorescence of all samples followed a sigmoidal curve with distinguishable lag, growth and stationary phases (Fig. 3e). However, the polymerization lag phases for CsgA-Mfp3 (unmodified or modified) and Mfp5-CsgA (unmodified or modified) were typically shorter than that for CsgA, suggesting that the fusion of Mfp domains to CsgA accelerates amyloid formation. This observation is consistent with the fly-casting mechanism, which postulates that a relatively unstructured protein can have a greater 'capture radius' and enhance the rate of intermolecular association[24]. Furthermore, partial conversion of tyrosine into DOPA in modified proteins shortened the time required to reach the stationary phase, implying a higher fibre formation rate in modified proteins (Fig. 3e).

The formation of long fibres was confirmed for all proteins with transmission electron microscopy (TEM), with no apparent differences in morphology and fibre length (Fig. 3f). However, the mean diameters of the three types of functionalized fibre in both unmodified and modified forms were three to five times larger than that of CsgA (Fig. 3f). In particular, the mean diameter of modified (CsgA-Mfp3)-co-(Mfp5-CsgA) copolymer fibres reached as high as ~50 nm, which is noticeably larger than the diameters of fibres composed of the unmodified copolymer and both unmodified and modified samples of CsgA-Mfp3 and Mfp5-CsgA. Note that all instances of the copolymer described hereafter were assembled from 1:1 molar ratios of CsgA-Mfp3:Mfp5-CsgA, unless otherwise noted. We believe that this increased diameter arises from additional intermolecular associations between the Mfp3 and Mfp5 domains in the copolymer construct. Circular dichroism studies (Supplementary Fig. 14) indicated that the fibres were generally rich in β-sheet secondary structure in solution, in agreement with molecular-dynamics modelling (Fig. 2). Interestingly, all of the unmodified and modified proteins, either upon incubation of freshly made soluble proteins over existing nanofibre seeds or upon incubation at high solution concentrations, assembled into larger fibre bundles and even thick hierarchical films composed of fibrils (Supplementary Figs 15, 16).

Intrinsic fluorescence of adhesive fibres

One remarkable feature of the adhesive fibres is that they all exhibited intrinsic fluorescence signatures in the visible spectrum range (Fig. 4a). Adhesive biomaterials that display intrinsic fluorescence may be useful for biological and imaging applications, similar to photoluminescent materials[25]. The unmodified adhesive fibres displayed higher fluorescence intensities than their modified counterparts when measured in bulk fibre bundles (Fig. 4a). These observations were in agreement with fluorescence quantum yields (Q, in %) determined by the Williams comparative method[26] (Fig. 4a, Supplementary Fig. 17). Among the unmodified fibres, Mfp5-CsgA had the highest Q-value of 4.2%, followed by 3.9% for the (CsgA-Mfp3)-co-(Mfp5-CsgA) copolymer and 2.8% for CsgA-Mfp3. However, for the modified fibres, the Q-values followed an opposite trend, with 1.9, 2.1 and 2.6% for Mfp5-CsgA, copolymer, and CsgA-Mfp3, respectively. Both unmodified and modified hybrid adhesive fibres had approximately two to four times higher Q-values than CsgA control fibres. Spectral analysis revealed that the excitation maxima for Mfp5-CsgA (unmodified or modified), CsgA-Mfp3 (unmodified or modified), copolymer (unmodified or

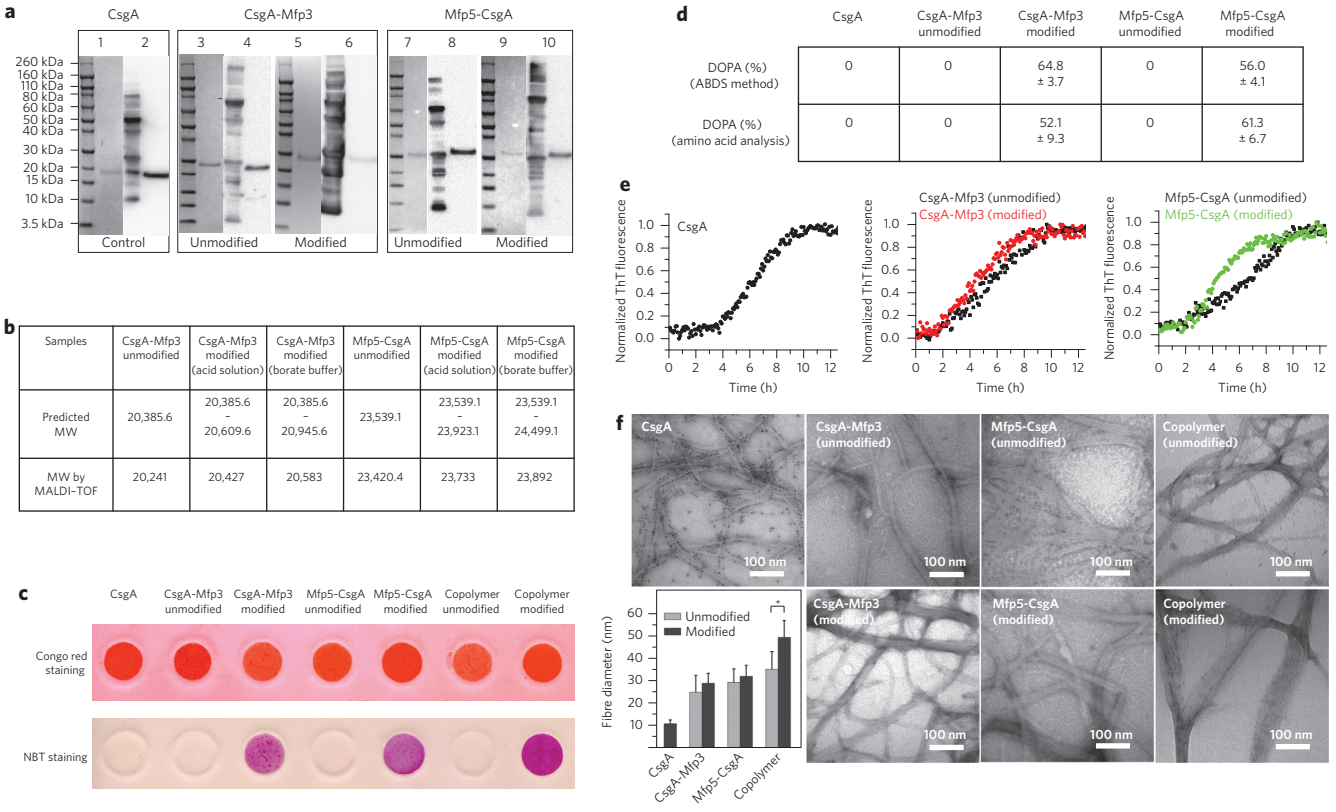

Figure 3 | Purification, *in vitro* self-assembly and characterization of CsgA, CsgA-Mfp3, Mfp5-CsgA and (CsgA-Mfp3)-co-(Mfp5-CsgA) fibres. **a**, Coomassie-stained SDS-PAGE gels and western blots with anti-His antibodies confirm purification of the expressed proteins by cobalt-resin columns. Lanes 1, 3, 5, 7 and 9 present data from SDS-PAGE, and lanes 2, 4, 6, 8 and 10 present corresponding data from western blots. **b**, MALDI-TOF confirms the molecular weights of CsgA-Mfp3 (unmodified and modified) and Mfp5-CsgA (unmodified and modified), which are consistent with predicted molecular weights. **c**, The CR assay confirms the amyloidogenic features of all fibres, and the NBT assay detects DOPA residues in modified fibres only. **d**, Quantitative analysis of DOPA residues in modified samples by ABDS analysis and AAA ($N = 3$). **e**, ThT assay, revealing the kinetics of amyloid formation for CsgA, CsgA-Mfp3 (unmodified and modified) and Mfp5-CsgA (unmodified and modified). **f**, TEM images of purified CsgA, CsgA-Mfp3 (unmodified and modified), Mfp5-CsgA (unmodified and modified) and (CsgA-Mfp3)-co-(Mfp5-CsgA) (unmodified and modified) solutions after three-day incubations at 4 °C demonstrate the formation of self-assembled fibres in all cases. CsgA-Mfp3, Mfp5-CsgA and (CsgA-Mfp3)-co-(Mfp5-CsgA) fibres all had larger diameters than CsgA fibres based on measurements from TEM images. Significant differences were detected between unmodified and modified (CsgA-Mfp3)-co-(Mfp5-CsgA) fibres, but no significant differences were found among unmodified and modified fibres of the other two types ($^*P < 0.05$). Error bars represent s.d. of the fibre diameters ($N = 50$). The copolymer refers to fibre structures formed via copolymerization of CsgA-Mfp3 and Mfp5-CsgA at a molar ratio of 1:1 (15 μM:15 μM) in solution.

modified) and CsgA fibres were near 318, 312, 315 and 306 nm, respectively, and the emission maxima were close to 378 nm for all constructs (Fig. 4b). Interestingly, when excited at different wavelengths, the adhesive fibres emitted fluorescence that could be detected with a wide range of filters with fluorescence microscopy, ranging from blue to red (Supplementary Fig. 18), in agreement with the spectral results (Fig. 4c). In addition, fluorescence was detected in aged solutions, but not in freshly made solutions, implying that fibre formation is a precondition for fluorescence (Fig. 4d).

Collectively, we suggest that electron delocalization via hydrogen bonds within ordered β-sheet structures[27] and the high percentage of aromatic side chains may both contribute to the intrinsic fluorescence signatures of our hybrid adhesive fibres. The higher fluorescence intensity of unmodified Mfp5-CsgA may arise from its higher fluorescent aromatic residue content (12.5%) compared with CsgA-Mfp3 (10.8%) and CsgA (5.8%), respectively. The decrease in fluorescence intensity within modified fibres versus their unmodified counterparts might be associated with partial conversation of tyrosine residues to DOPA, as the fluorescence quantum yield of DOPA residue (0.09)[28] is lower than that of tyrosine (0.14)[29] in acid-neutral solutions and is further substantially reduced in conjugate base forms (for example, with deprotonation of the phenolic hydroxyl group)[28]. Decreased fluorescence in modified fibres might also be related to fluorescence quenching due to auto-oxidation or potential crosslinking[30].

Underwater adhesion performance of adhesive fibres

To assess the underwater adhesion performance of the adhesive fibres, we used the atomic force microscopy (AFM) colloidal probe technique[31] (Fig. 5a). This technique essentially measures the asymmetric adhesion of fibres, which pre-bind firmly to mica and bind to the AFM tip surface temporarily during measurement. The AFM tips used in this study included silica, gold and polystyrene (PS) surfaces, which were chosen as representative inorganic, metal and polymeric surfaces. Proteins were deposited and adsorbed on clean mica surfaces under buffered aqueous conditions with a wide range of pH values. Fibrous structures were found covering the mica surfaces after 1 h of adsorption (Fig. 5a, Supplementary Fig. 19). To comprehensively understand the adhesive behaviour of the fibres we performed both force-mapping-mode and continuous-measurement-mode studies, which were consistent with one another (Fig. 5b,c). Thus, we concluded that our fibres exhibited repeatable adhesion properties (rather than just a single adhesion

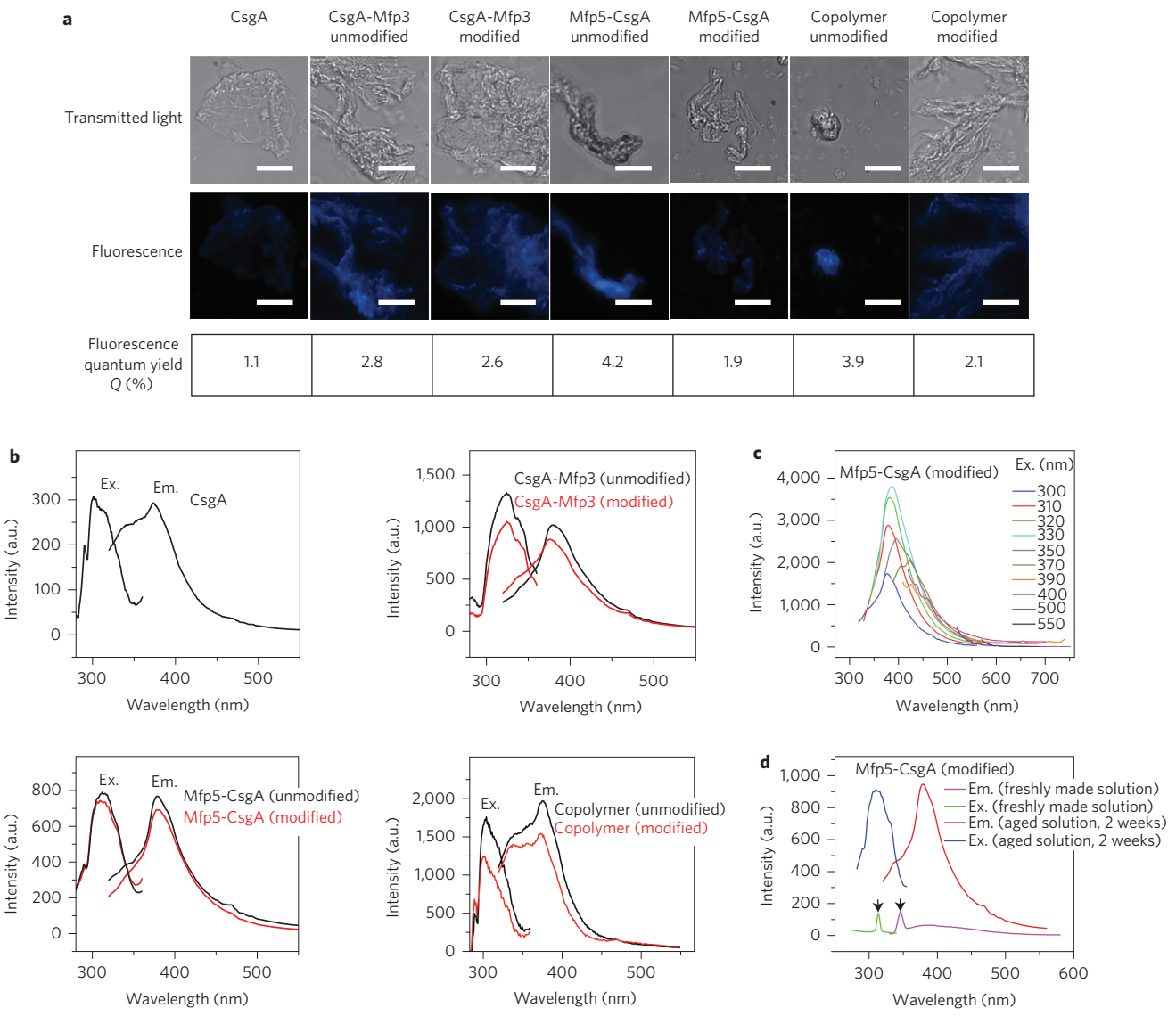

Figure 4 | Intrinsic fluorescence of CsgA, CsgA-Mfp3, Mfp5-CsgA and (CsgA-Mfp3)-co-(Mfp5-CsgA) copolymer fibres. a, Comparison of intrinsic blue fluorescence of CsgA with both unmodified and modified samples of CsgA-Mfp3, Mfp5-CsgA and copolymer fibres, detected with fluorescence microscopy with an enhanced blue fluorescent protein fluorescence filter (excitation wavelength, 385 nm; emission wavelength, 448 nm). Corresponding fluorescence quantum yields (ratios of photons absorbed to photons emitted) were determined following the standard Williams comparative method (Supplementary Fig. 17). Scale bars, 20 μm. **b**, Excitation (Ex.) and emission (Em.) spectra of CsgA, CsgA-Mfp3 (unmodified and modified), Mfp5-CsgA (unmodified and modified) and copolymer (unmodified and modified) fibres. Excitation spectra were measured with the emission wavelength fixed at 375 nm, while emission spectra were measured with the excitation wavelength fixed at 300 nm. **c**, Emission spectra of modified Mfp5-CsgA fibres measured at different excitation (Ex.) wavelengths. **d**, Excitation and emission spectra for freshly made Mfp5-CsgA solutions as well as Mfp5-CsgA solutions aged for 2 weeks. No fluorescence features were detected with freshly made Mfp5-CsgA. The two peaks in the curves for freshly made Mfp5-CsgA could be assigned to Raman peaks for water (arrows)[50]. In contrast, significant fluorescence signals were detected in solution after Mfp5-CsgA solutions were aged for two weeks, during which time fibres formed. The fluorescence signal of aged solutions almost covered the Raman peaks assigned to water. The copolymer refers to fibre structures that formed via copolymerization of CsgA-Mfp3 and Mfp5-CsgA at a molar ratio of 1:1 (15 μM:15 μM) in solution.

event) and that the adhesion characteristics were indeed dependent on the specific adhesive fibres studied (Figs 5b,c and 6).

The stability of adhesion was assessed on unmodified and modified Mfp5-CsgA fibres under aqueous conditions with different pH values (pH 2.5, 5.0, 7.0 and 10.0) (Fig. 5d). Both unmodified and modified Mfp5-CsgA fibres maintained adhesion under acidic and neutral conditions (pH 2.5–7.0). Surprisingly, both modified and unmodified Mfp5-CsgA fibres still exhibited considerable levels of adhesion, even under basic conditions (pH 10.0). Similar trends were observed for the other fibre types (data not shown). These data contrast with previous findings that reported that soluble and non-fibrous *Mytilus edulis* foot protein-5 (Mefp5) had a threefold lower adhesion energy[32] at pH 5.5 than at pH 2.6 as well as studies showing that adhesion by Mfp3 and Mfp5 is almost completely abolished when exposed to slightly basic conditions ($pH \geq 7.5$)[32,33]. These results suggest that our adhesive fibres generally exhibit better tolerance to auto-oxidation compared with previous reports on Mfps alone, possibly arising from the protective effects of hydrophobic aromatic residues and the general hydrophobic features of amyloid fibres[34,35]. In particular, partial conversion (~50–70%) of tyrosine to DOPA in our adhesive proteins may resemble the so-called Mfp3 'slow' variant, which is composed of both DOPA and more hydrophobic tyrosine residues and was recently reported to preserve significant

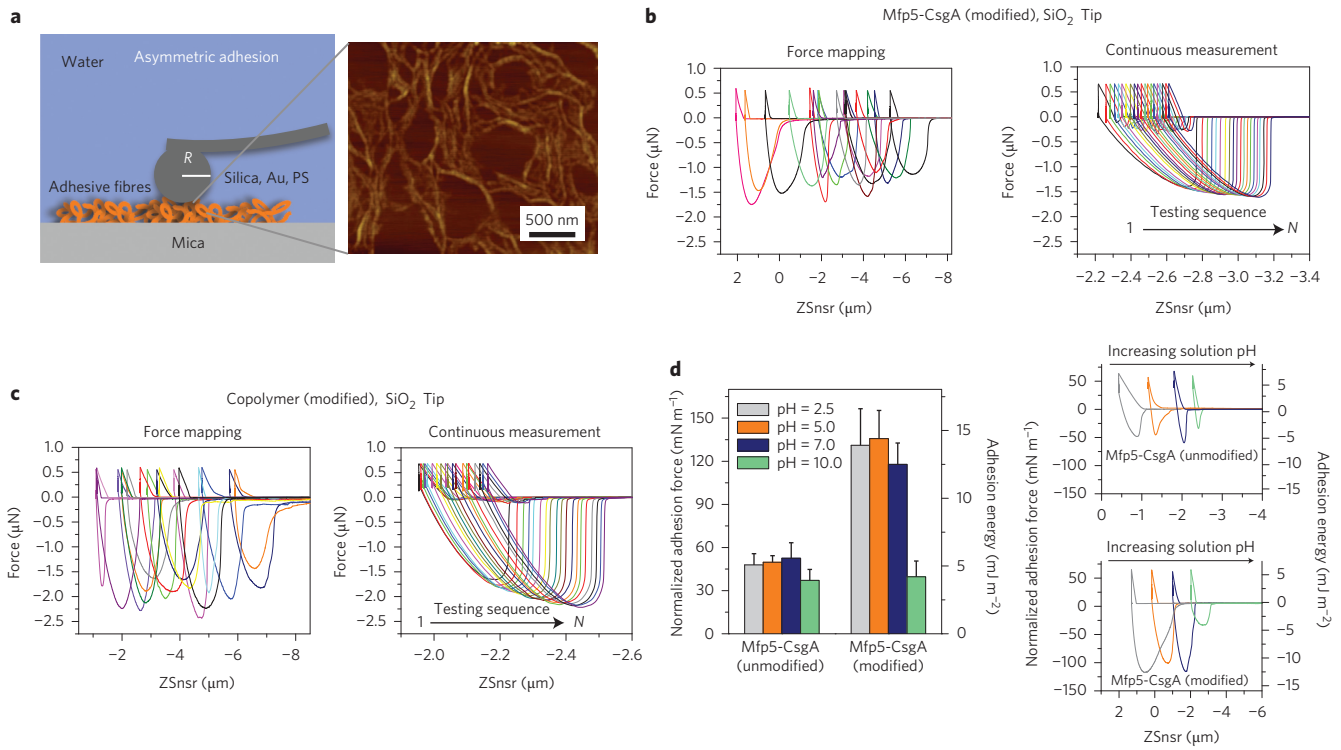

Figure 5 | Adhesion force measurements and adhesion stability of hybrid adhesive fibres determined by the AFM colloidal probe technique. a, Schematic of a spherulitic particle AFM probe (R = 10 μm for silica and gold tips, R = 12.5 μm for PS tips) used to measure the asymmetric adhesion of nanofibres deposited on smooth mica surfaces in the presence of buffered aqueous solutions. Right: Representative AFM image showing modified Mfp5-CsgA fibres 1 h after deposition on a mica surface. **b**, Representative adhesion force curves collected with the force mapping mode and continuous measurement mode for modified Mfp5-CsgA samples measured with silica tips. The force mapping mode enables statistical analyses of fibre adhesion based on the random measurement of spots containing nanofibres on the mica surfaces with a scanning range of 20–100 μm. The continuous measurement mode includes 20 continuous measurements on the same specific fibre spot, thus enabling assessment of the cyclic behaviour of contacts between nanofibres and probes. **c**, Representative adhesion force curves collected through the force mapping mode and continuous measurement mode for modified (CsgA-Mfp3)-co-(Mfp5-CsgA) copolymer (1:1 ratio) measured with silica tips. **d**, Adhesion stability of Mfp5-CsgA (unmodified and modified) fibres measured with silica tips in the presence of buffered aqueous solutions of varied pH values (N = 64). Right: Representative adhesion curves for both unmodified and modified samples of Mfp5-CsgA. Note that the adhesion force curves are plotted as force–displacement curves. The x axis, ZSnsr (Z sensor), represents the displacement between the sample surface and the resting position of the cantilever (rather than the actual distance between the sample surface and the AFM tip).

adhesion even at pH 7.0 due to hydrophobicity compensation for DOPA oxidation[33].

We also compared the adhesive behaviours of different functionalized adhesive fibres (Fig. 6). For the same protein, modified fibres always displayed higher adhesion (at least a two- to threefold increase) compared with unmodified fibres (Fig. 6a), independent of the AFM tips (silica, gold and PS) used. These data suggest that DOPA residues in the self-assembled nanofibres contribute significantly to underwater adhesion. However, unmodified fibres also displayed higher adhesion than the CsgA control, implying that features of Mfp domains other than DOPA can participate in underwater adhesion (Fig. 6a). A further comparison of different modified adhesive fibres measured under the same conditions with the same type of tips indicated that adhesion performance had the following general trend, independent of the AFM tip used: (CsgA-Mfp3)-co-(Mfp5-CsgA) copolymer > Mfp5-CsgA > CsgA-Mfp3 > CsgA. Among the three tips, the most obvious trend was observed with silica. Testing with silica tips showed very high underwater adhesion for modified Mfp5-CsgA and copolymer fibres (Figs 5b,c and 6a). Specifically, modified Mfp5-CsgA fibres had a normalized adhesion force (force/radius, F/R) and adhesion energy (E_{ad}) of 136 mN m^{-1} and 14.4 mJ m^{-2}, respectively. Of note, the adhesion energy of Mfp5-CsgA fibres was three times greater than the reported adhesion energy for recombinant Mfp5 alone under the same conditions[9], and was three times higher than that for Mefp5, the most adhesive mussel protein reported to date, at pH ≈ 5.0 (ref. 32).

Interestingly, the (CsgA-Mfp3)-co-(Mfp5-CsgA) copolymer (1:1 ratio) had significantly higher adhesion than Mfp5-CsgA and CsgA-Mfp3 when measured with silica tips ($P < 0.01$). Specifically, the copolymer fibres demonstrated values of F/R = 197.5 mN m^{-1} and E_{ad} = 20.9 mJ m^{-2}. These are approximately two to three times higher than for modified CsgA-Mfp3 measured under the same conditions (Fig. 6a). Moreover, copolymers with a CsgA-Mfp3:Mfp5-CsgA monomer ratio of 1:1 displayed higher adhesion than copolymers assembled from monomer ratios of 3:7 or 7:3 (Supplementary Fig. 23). To our knowledge, the (CsgA-Mfp3)-co-(Mfp5-CsgA) copolymer (1:1 ratio) fibres exhibited the strongest underwater adhesion among all known bio-derived and bio-inspired protein-based underwater adhesives reported to date[2,5,32,36]. We hypothesize that amyloid fibre structures enable large surface areas for contact, with multiple disordered Mfp domains on fibre surfaces interacting to achieve enhanced ultra-strong underwater adhesion. This hypothesis is supported by the larger mean fibre diameters of copolymer-based fibres compared with fibres assembled from individual proteins, as noted above (Fig. 3f).

We also compared how different AFM tips with varied surface energies affect the adhesive behaviours of the same types of protein (Fig. 6b). Among all the adhesive proteins studied, significant adhesion differences between tips were only found in

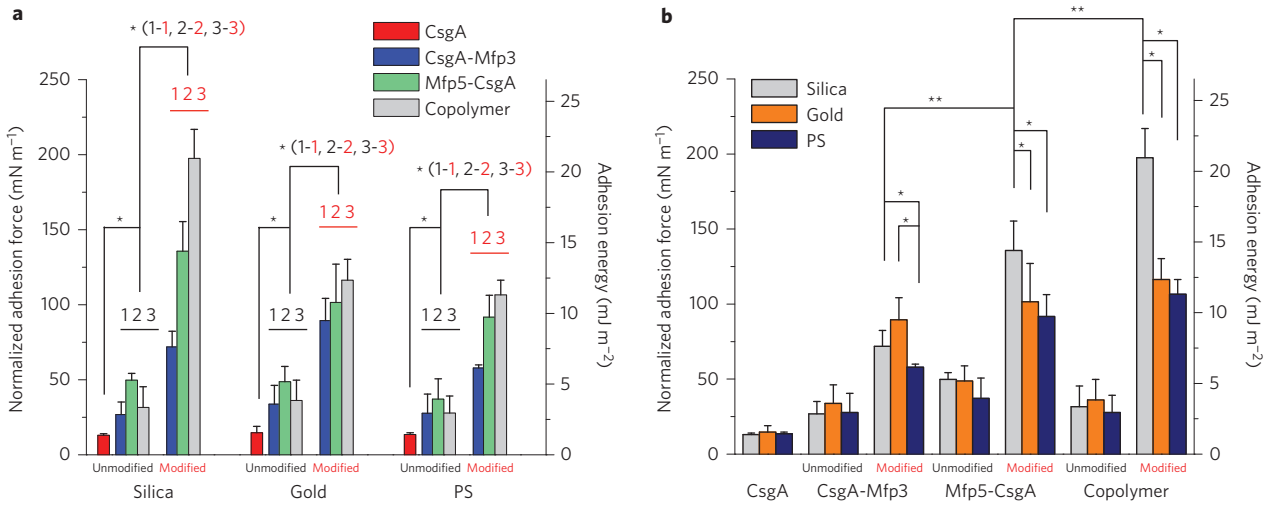

Figure 6 | Comparison of adhesion performances of different functionalized adhesive fibres with different AFM tips. a, Comparison of adhesion forces (normalized force (force/radius) and adhesion energies ($E_{ad} = F/3\pi R$)) for CsgA (control) with unmodified and modified versions of functionalized adhesive fibres, measured with silica, gold and PS tips. **b**, Effects of AFM tips with varied surface energies on the adhesion properties of all adhesive fibres, including CsgA and unmodified and modified versions of CsgA-Mfp3, Mfp5-CsgA and (CsgA-Mfp3)-co-(Mfp5-CsgA) copolymer (1:1 ratio). $^*P < 0.05$, $^{**}P < 0.01$. Error bars indicate s.d. For each statistical analysis $N = 64$ (4 groups × 16 random spots/group). All data in this figure were measured with the force mapping mode in phosphate buffer at pH 5.0. In **a** and **b**, the same data are plotted in two different formats to enable convenient comparisons. In **a**, the asterisk (*) for CsgA versus unmodified fibres indicates three independent tests between CsgA and the three different fibres, and 1-1, 2-2 and 3-3 refer to comparisons between unmodified and modified samples for the same type of fibre.

tyrosinase-modified samples of CsgA-Mfp3, Mfp5-CsgA and copolymer (1:1 ratio) (Fig. 6b, Supplementary Figs 25–27). Specifically, for modified CsgA-Mfp3, the general trend of adhesion was silica ≈ gold > PS ($P < 0.05$). For modified Mfp5-CsgA and copolymer (1:1 ratio), the trend was silica > gold ≈ PS ($P < 0.05$). Both CsgA-Mfp3 and Mfp5-CsgA have basic pIs (~9.0–9.4) and are therefore positively charged under acidic and neutral conditions and can effectively bind to negatively charged SiO_2 surfaces. Hydrogen bonding (between hydroxyl or amine groups on proteins and oxygen atoms on SiO_2), bidentate hydrogen bonding by DOPA, or hydrogen bonds coupled with coordinate bonds between DOPA and silica could contribute to the strong adhesion of fibres with SiO_2 surfaces[36–38]. In contrast, the adhesion of fibres to PS and gold surfaces could be mainly due to hydrophobic interactions, with additional cation–π interactions or π–π interactions probably associated with PS surfaces[36,38]. Previous studies in which adhesion was measured with a surface force apparatus revealed that non-fibrous Mfp3 and Mfp5 molecules exhibited the highest adhesion to PS among four substrates (silica, PS, mica and poly(methylmethacrylate)) with short contact times and had the same level of adhesion to silica and PS with longer contacts[36]. In contrast, we found that stronger adhesion was found with silica tips and tyrosinase-modified fibres. These observations suggest that, other than providing a high surface area for contact, the amyloid domains of our adhesive fibres may modulate how the Mfp domains interact with the substrates and achieve different adhesion levels.

Conclusions

We have demonstrated a modular genetic strategy for the design of bio-inspired hybrid fibres for underwater adhesives. Our strategy combines the properties of amyloids and DOPA-containing mussel-foot proteins, two natural adhesives used as building blocks. The resulting fibres have hierarchical structures and multifunctional properties, such as strong wet bonding strength, material robustness, enhanced stability and intrinsic fluorescence. In particular, the underwater adhesion energy reached 20.9 mJ m^{-2}, which is 1.5 times greater than the maxima of all bio-derived and bio-inspired protein-based underwater adhesives reported to date. We envision that engineering the complex self-assembly of multiple biomolecular building blocks is a promising strategy to enhance the properties of bio-inspired and bio-mimetic materials. As demonstrated in the present work, this strategy can be particularly successful for amyloid-based materials, which have attractive properties[16,19] and have been discovered in several biological settings[39].

Our approach builds upon decades of molecular biology and functional genomics research, which has resulted in a diverse library of functional biomolecules that are ripe for incorporation into new bio-inspired molecular materials using synthetic-biology tools. These strategies have already enabled the rational and high-throughput assembly of biological components[40], have been used to produce living functional materials[41], self-assembling nanostructures[42] and muscle-mimetic biomaterials[43], and have been used to design biological devices with predictable, useful and novel functions[44,45]. Furthermore, recent advances in *in vitro*[46] and cellular expression systems[47] that can incorporate unnatural amino acids may open up new capabilities in materials design.

Methods

Gene construction and sequencing. Mussel foot protein-3 or -5 (*mfp3* or *mfp5*) gene sequences were synthesized by Integrated DNA Technologies. Recombinant genes combining *csgA* and *mfp3* or *mfp5* with appended C-terminal poly-histidine tags were constructed using isothermal Gibson assembly and cloned into pET-11d expression vectors. Plasmid construct sequences were confirmed by restriction digest, and sequencing was performed by Genewiz. The primers used for Polymerase Chain Reaction and the parts that constitute the plasmids are described in Supplementary Table 1. Plasmid maps are described in Supplementary Fig. 2. Sequencing results for *csgA*, *csgA-mfp3* and *mfp5-csgA* are presented in Supplementary Figs 3, 4 and 5, respectively.

Molecular dynamics simulations. The initial model for the CsgA moiety was constructed by threading the CsgA amino-acid sequence onto a structure of an amyloid β42 amyloid fibril using Modeller (PDB ID 2BEG)[48]. Molecular dynamics simulations were run for a total of 1 μs and 200 ns for the monomeric proteins and fibrils, respectively. Further details on model construction are provided in Supplementary Section 2.

Expression, purification and characterization of adhesive proteins. Detailed information about protein expression, purification and *in vitro* post-translational modification are described in Supplementary Section 5. Purified proteins were assayed with SDS-PAGE, western blotting, MALDI–TOF mass spectrometry and

amino acid analysis (AAA). The general amyloid features of all adhesive fibres were detected with a Congo red (CR) assay. DOPA residues in modified proteins were qualitatively detected by NBT staining and quantitatively analysed with ABDS analysis, supported by AAA. The kinetics of amyloid fibre formation was assessed with a ThT assay. The specific experimental protocols are described in detail in Supplementary Sections 5–10 and Supplementary Figs 7–14.

Morphology characterization. The morphology of fibres was assessed with TEM and AFM imaging. Bright-field TEM images were collected on an FEI Tecnai G2 F20 S/TEM operating at an accelerating voltage of 200 kV after staining the samples with uranyl-acetate or gold nanoparticles. Tapping-mode AFM was performed on an Asylum MFP-3D AFM (Asylum Research) using Veecoprobes Sb-doped Si cantilevers ($\rho = 0.01$–0.025Ωcm, $k = 40$ N m^{-1}, $\nu \approx 300$ kHz).

Fluorescence microscopy, fluorescence spectra and fluorescence quantum yields. Fluorescence images were recorded on a Nikon Ti-E PFS fluorescence microscope coupled with an Olympus IX70 inverted microscope frame. Ultraviolet–visible (UV–Vis) absorption spectra were recorded with a CARY-6000i spectrophotometer. Fluorescence emission and excitation spectra were measured using a FluoroLog 3 spectrometer manufactured by HORIBA Jobin Yvon. The fluorescence quantum yields (Q, in %) of adhesive fibres were assessed with the Williams comparative method[26] using a standard blue fluorophore (Coumarin 102) with a known quantum yield of $Q = 76.4\%$ in ethanol. Detailed information about the determination of fluorescence quantum yields is provided in Supplementary Section 14 and Supplementary Fig. 17.

Adhesion force measurements by AFM. AFM force measurements were carried out using an Asylum MFP-3D AFM (Asylum Research) mounted on top of an Olympus IX51 inverted optical microscope for visualizing and manually positioning regions to be probed. Force measurements (force–distance curves) were conducted at a rate of 0.3–2.0 Hz, using Si_3N_4 or Si cantilevers modified with a glass sphere (radius, 10 μm), a glass sphere coated with gold layers (radius, 10 μm) or a polystyrene sphere (radius, 12.5 μm) (Novascan), with calibrated spring constants between 0.6 and 14 N m^{-1}. Both force-mapping-mode and continuous-measurement-mode methods were used in this study. All adhesion plots shown in the figures were based on data collected from the force mapping mode, and confirmed with the continuous measurement mode. More detailed information about adhesion force measurements is provided in Supplementary Section 15 and Supplementary Figs 21–35.

Statistics. Data are presented as mean ± s.d. (standard deviation). The values of s.d. were calculated based on at least three replicates (for force measurements, this refers to at least $4 \times 16 = 64$ force curves for each type of protein). A Student's t-test was used to compare data sets, and P-values less than 0.01 and 0.05 were considered statistically significant between two marked groups or samples.

Received 28 October 2013; accepted 14 August 2014; published online 21 September 2014

References

1. Dolgin, E. The sticking point. *Nature Med.* **19,** 124–125 (2013).
2. Lee, B. P., Messersmith, P. B., Israelachvili, J. N. & Waite, J. H. Mussel-inspired adhesives and coatings. *Annu. Rev. Mater. Res.*, **41,** 99–132 (2011).
3. Brubaker, C. E. & Messersmith, P. B. The present and future of biologically inspired adhesive interfaces and materials. *Langmuir* **28,** 2200–2205 (2012).
4. Stewart, R. J., Ransom, T. C. & Hlady, V. Natural underwater adhesives. *J. Polym. Sci. B* **49,** 757–771 (2011).
5. Stewart, R. J. Protein-based underwater adhesives and the prospects for their biotechnological production. *Appl. Microbiol. Biotechnol.* **89,** 27–33 (2011).
6. Yin, M., Yuan, Y., Liu, C. S. & Wang, J. Development of mussel adhesive polypeptide mimics coating for *in-situ* inducing re-endothelialization of intravascular stent devices. *Biomaterials* **30,** 2764–2773 (2009).
7. Brubaker, C. E., Kissler, H., Wang, L. J., Kaufman, D. B. & Messersmith, P. B. Biological performance of mussel-inspired adhesive in extrahepatic islet transplantation. *Biomaterials* **31,** 420–427 (2010).
8. Matos-Perez, C. R., White, J. D. & Wilker, J. J. Polymer composition and substrate influences on the adhesive bonding of a biomimetic, cross-linking polymer. *J. Am. Chem. Soc.* **134,** 9498–9505 (2012).
9. Hwang, D. S., Yoo, H. J., Jun, J. H., Moon, W. K. & Cha, H. J. Expression of functional recombinant mussel adhesive protein Mgfp-5 in *Escherichia coli*. *Appl. Environ. Microbiol.* **70,** 3352–3359 (2004).
10. Kamino, K., Nakano, M. & Kanai, S. Significance of the conformation of building blocks in curing of barnacle underwater adhesive. *FEBS J.* **279,** 1750–1760 (2012).
11. Kamino, K. Underwater adhesive of marine organisms as the vital link between biological science and material science. *Marine Biotechnol.* **10,** 111–121 (2008).
12. Anika, S. in *The Functional Fold: Amyloid Structures in Nature* (ed. Mostaert, S. J. A.) 131–146 (Pan Stanford, 2012).
13. Barlow, D. E. *et al.* Characterization of the adhesive plaque of the barnacle *Balanus amphitrite*: amyloid-like nanofibrils are a major component. *Langmuir* **26,** 6549–6556 (2010).
14. Wasmer, C. *et al.* Amyloid fibrils of the HET-s(218–289) prion form a beta solenoid with a triangular hydrophobic core. *Science* **319,** 1523–1526 (2008).
15. Sawaya, M. R. *et al.* Atomic structures of amyloid cross-beta spines reveal varied steric zippers. *Nature* **447,** 453–457 (2007).
16. Knowles, T. P. J. & Buehler, M. J. Nanomechanics of functional and pathological amyloid materials. *Nature Nanotech.* **6,** 469–479 (2011).
17. Knowles, T. P. *et al.* Role of intermolecular forces in defining material properties of protein nanofibrils. *Science* **318,** 1900–1903 (2007).
18. Chapman, M. R. *et al.* Role of *Escherichia coli* curli operons in directing amyloid fiber formation. *Science* **295,** 851–855 (2002).
19. Knowles, T. P. J., Oppenheim, T. W., Buell, A. K., Chirgadze, D. Y. & Welland, M. E. Nanostructured films from hierarchical self-assembly of amyloidogenic proteins. *Nature Nanotech.* **5,** 204–207 (2010).
20. Li, C. X., Adamcik, J. & Mezzenga, R. Biodegradable nanocomposites of amyloid fibrils and graphene with shape-memory and enzyme-sensing properties. *Nature Nanotech.* **7,** 421–427 (2012).
21. Waite, J. H. & Benedict, C. V. Assay of dihydroxyphenylalanine (dopa) in invertebrate structural proteins. *Methods Enzymol.* **107,** 397–413 (1983).
22. Paz, M., Flückiger, R., Boak, A., Kagan, H. & Gallop, P. M. Specific detection of quinoproteins by redox-cycling staining. *J. Biol. Chem.* **266,** 689–692 (1991).
23. Wang, X., Zhou, Y., Ren, J-J., Hammer, N. D. & Chapman, M. R. Gatekeeper residues in the major curlin subunit modulate bacterial amyloid fiber biogenesis. *Proc. Natl Acad. Sci. USA* **107,** 163–168 (2010).
24. Sugase, K., Dyson, H. J. & Wright, P. E. Mechanism of coupled folding and binding of an intrinsically disordered protein. *Nature* **447,** 1021–1025 (2007).
25. Yang, J. *et al.* Development of aliphatic biodegradable photoluminescent polymers. *Proc. Natl Acad. Sci. USA* **106,** 10086–10091 (2009).
26. Williams, A. T. R., Winfield, S. A. & Miller, J. N. Relative fluorescence quantum yields using a computer-controlled luminescence spectrometer. *Analyst* **108,** 1067–1071 (1983).
27. Del Mercato, L. L. *et al.* Charge transport and intrinsic fluorescence in amyloid-like fibrils. *Proc. Natl Acad. Sci. USA* **104,** 18019–18024 (2007).
28. Smith, G. J. The fluorescence of dihydroxyphenylalanine: the effects of protonation–deprotonation. *Color. Technol.* **115,** 346–349 (1999).
29. Chen, R. F. Fluorescence quantum yields of tryptophan and tyrosine. *Anal. Lett.* **1,** 35–42 (1967).
30. Al-Hilaly, Y. K. *et al.* A central role for dityrosine crosslinking of amyloid-β in Alzheimer's disease. *Acta Neuropathol. Commun.* **1,** 83 (2013).
31. Leite, F. & Herrmann, P. Application of atomic force spectroscopy (AFS) to studies of adhesion phenomena: a review. *J. Adhes. Sci. Technol.* **19,** 365–405 (2005).
32. Danner, E. W., Kan, Y. J., Hammer, M. U., Israelachvili, J. N. & Waite, J. H. Adhesion of mussel foot protein Mefp-5 to mica: an underwater superglue. *Biochemistry* **51,** 6511–6518 (2012).
33. Wei, W., Yu, J., Broomell, C., Israelachvili, J. N. & Waite, J. H. Hydrophobic enhancement of dopa-mediated adhesion in a mussel foot protein. *J. Am. Chem. Soc.* **135,** 377–383 (2012).
34. Wu, C., Lim, J. Y., Fuller, G. G. & Cegelski, L. Quantitative analysis of amyloid-integrated biofilms formed by uropathogenic *Escherichia coli* at the air–liquid interface. *Biophys. J.* **103,** 464–471 (2012).
35. Goulter-Thorsen, R., Taran, E., Gentle, I., Gobius, K. & Dykes, G. CsgA production by *Escherichia coli* O157: H7 alters attachment to abiotic surfaces in some growth environments. *Appl. Environ. Microbiol.* **77,** 7339–7344 (2011).
36. Lu, Q. *et al.* Adhesion of mussel foot proteins to different substrate surfaces. *J. R. Soc. Interface* **10,** 20120759 (2013).
37. Yu, J. *et al.* Adaptive hydrophobic and hydrophilic interactions of mussel foot proteins with organic thin films. *Proc. Natl Acad. Sci. USA* **110,** 15680–15685 (2013).
38. Li, Y., Qin, M., Li, Y., Cao, Y. & Wang, W. Single molecule evidences for the adaptive binding of DOPA to different wet surfaces. *Langmuir* **30,** 4358–4366 (2014).
39. Fowler, D. M., Koulov, A. V., Balch, W. E. & Kelly, J. W. Functional amyloid—from bacteria to humans. *Trends Biochem. Sci.* **32,** 217–224 (2007).
40. Weber, W. & Fussenegger, M. Emerging biomedical applications of synthetic biology. *Nature Rev. Genet.* **13,** 21–35 (2012).
41. Chen, A. Y. *et al.* Synthesis and patterning of tunable multiscale materials with engineered cells. *Nature Mater.* **13,** 515–523 (2014).
42. Sinclair, J. C., Davies, K. M., Venien-Bryan, C. & Noble, M. E. M. Generation of protein lattices by fusing proteins with matching rotational symmetry. *Nature Nanotech.* **6,** 558–562 (2011).
43. Lv, S. *et al.* Designed biomaterials to mimic the mechanical properties of muscles. *Nature* **465,** 69–73 (2010).
44. Qian, L. & Winfree, E. Scaling up digital circuit computation with DNA strand displacement cascades. *Science* **332,** 1196–1201 (2011).
45. Auslander, S., Auslander, D., Muller, M., Wieland, M. & Fussenegger, M. Programmable single-cell mammalian biocomputers. *Nature* **487,** 123–127 (2012).

46. Hong, S. H. *et al.* Cell-free protein synthesis from a release factor 1 deficient *Escherichia coli* activates efficient and multiple site-specific non-standard amino acid incorporation. *ACS Synth. Biol.* **3,** 398–409 (2014).
47. Lajoie, M. J. *et al.* Genomically recoded organisms expand biological functions. *Science* **342,** 357–360 (2013).
48. Eswar, N. *et al.* Comparative protein structure modeling using Modeller. *Curr. Protoc. Bioinf.* 5.6.1–5.6.30 (2006).
49. Hwang, D. S. & Waite, J. H. Three intrinsically unstructured mussel adhesive proteins, mfp-1, mfp-2, and mfp-3: analysis by circular dichroism. *Protein Sci.* **21,** 1689–1695 (2012).
50. Lakowicz, J. R. *Principles of Fluorescence Spectroscopy* (Springer, 2009).

Acknowledgements

The authors thank A. Schwartzman for help in applying AFM colloid nanoparticle technology for measuring adhesive forces and H. Tavakoli Nia (Ortiz group, MIT) for initial discussions regarding this technology. The authors acknowledge help from the NERCE Biomolecule Production Laboratory (Harvard University) for producing part of the cell pellets for protein purification. The authors also thank the Whitehead Institute and the Biopolymers Laboratory in the David H. Koch Institute for Integrated Cancer Research and the Institute for Soldier Nanotechnologies for access to characterization equipment. This research was primarily supported by the Office of Naval Research (N000141310647). This work was also supported in part by the MRSEC Program of the National Science Foundation under award no. DMR-0819762. T.K.L. acknowledges support from the NIH New Innovator Award (1DP2OD008435). The molecular dynamics modelling used the computer cluster and corresponding materials based upon work supported by the National Science Foundation under award no. 0821391.

Author contributions

T.K.L. directed the research. C.Z. conceived the technical details and designed the experiments. C.Z. performed or participated in all the experiments. J.D. performed experiments in protein expression and purification. Z.D. assisted in collecting and analysing the fluorescence emission and excitation spectra. A.C. constructed the genes. C.M.S. and T.G. designed the simulations. T.G. performed the simulations. C.Z. and T.K.L. wrote the manuscript with help from all authors. All authors contributed to revising the manuscript.

Additional information

Supplementary information is available in the online version of the paper. Reprints and permissions information is available online at www.nature.com/reprints. Correspondence and requests for materials should be addressed to T.K.L.

Competing financial interests

T.K.L. and C.Z. have filed a patent disclosure with the MIT Technology Licensing Office on this work.